CHAPTER 5

APPLICATION OF PURE ZnO AND Nb-DOPED ZnO FOR USE AS PHOTOCATALYSTS

5.1 Introduction

ZnO is a well known to be one of the important photocatalysts because of its unique advantages, such as its low price, high photocatalytic activity, high stability and nontoxicity. According to these properties, ZnO has attracted a great deal of attention for use as a catalyst in photooxidation of organic pollutants [1–3]. The photocatalytic degradation of various organic compounds catalyzed by ZnO has been widely studied [4–9]. It has been suggested that ZnO is a low cost alternative photocatalyst to TiO_2 for removal of organics in aqueous solutions [10–19], as it has a similar band gap energy (3.2 eV) [20–21]. Bandgap energies of common semiconductors are given in Figure 5.1. Photocatalytic efficiency has been reported [22–26]. ZnO absorbs ultraviolet (UV) light through a process of electronic excitation between the valence band and conduction band. In conjunction with its high chemical stability and low toxicity, this property of ZnO renders its suitability for use as a UV-screening agent in a diverse range of applications, which include sunscreens and protective wood coatings. In such applications, ZnO is superior to TiO_2 due to its broader absorption of UV-light (ZnO absorbs both UVA and UVB whereas TiO_2 only absorbs UVA are shown in Figure 5.2) and its lower refractive index.

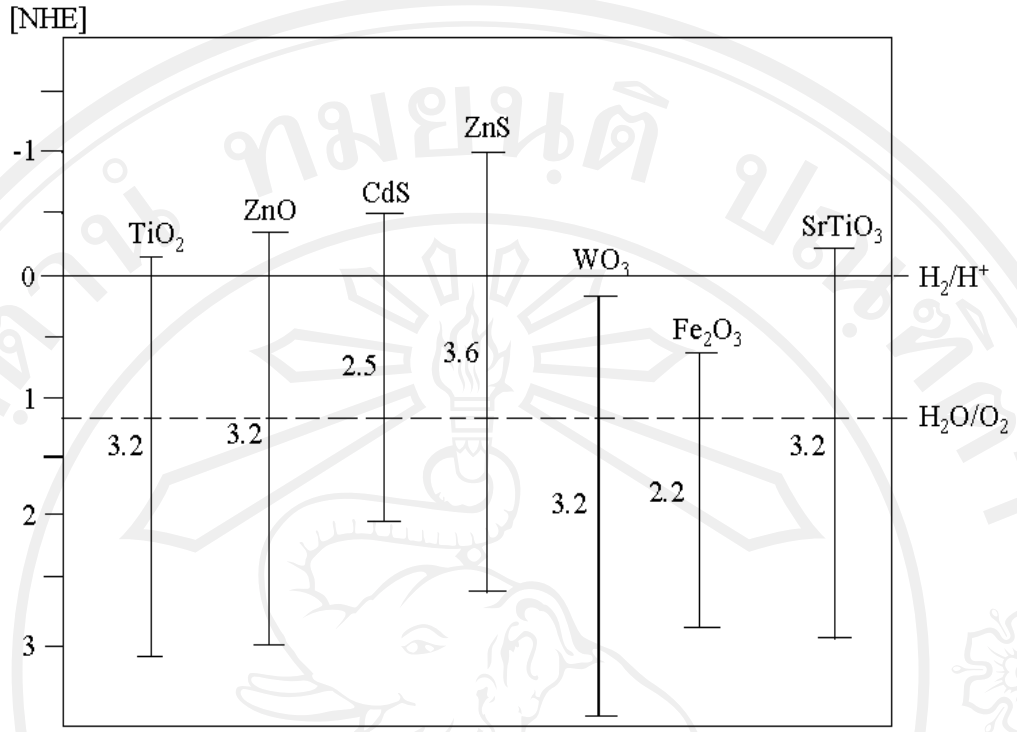

Figure 5.1 Bandgap energies for some common semiconductor materials at 0 K [27].

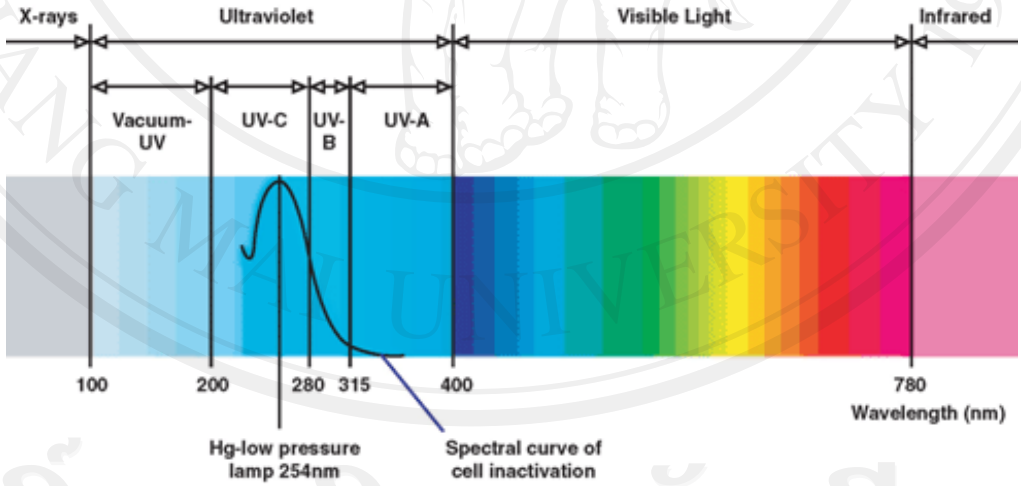

Figure 5.2 The eletromagnetic spectrum [28].

It is well known that the surface characteristic of ZnO determined by different fabrication processes can influence the photocatalytic property as well as the final

degradation efficiency. This suggested that the photocatalytic activities of ZnO are directly related to its preparation, particle size, morphology and dopant concentrations.

Various methods have been employed to prepare ultrafine ZnO. By using the flame spray technique, ultrafine ZnO particles with high surface area and controlled size and crystallinity can be obtained [29]. The process has been demonstrated as one-step dry synthesis of high surface area, and highly efficient noble metal catalysts allowing rapid production of nanomaterials and versatility in material compositions. These advantages prompted us to apply FSP for production of pure ZnO and Nb-doped ZnO nanoparticles as photocatalysts in the organic compounds degradation.

In order to obtain the highly effective ZnO photocatalyst, doping of metal ions into ZnO particles is usually performed, since the presence of metal dopants in ZnO crystalline matrix can significantly affect the photocatalytic activity, charge carrier recombination rate and interfacial electron transfer rate [30]. Various metal dopants, especially the transition metals (e.g. Co [31–33], Mn [33–34], Ti [35], La [36], Fe [37], Ni [38]) have been used and their photocatalytic activities have already been examined. However, to the best of our knowledge, the photocatalytic activity of Nb-doped ZnO has not been reported. The aim of this chapter is not only preparation of high surface area Nb-doped ZnO catalysts by FSP technique but also to investigate the catalytic performance of these materials on photodegradation of organic contaminants (i.e. ethanol, methanol, sucrose and glucose) under UVA irradiation.

5.1.1 Function and principles of photocatalysts [39–42]

Semiconductors are primary light absorbers. They are used in photocatalysis because of a favorable combination of electronic structure, light absorption properties, charge transport characteristics, and excited-state lifetimes [39]. The principal mechanism of a semiconductor photocatalytic reaction is as follows. When a photocatalytic surface is illuminated by light with energy equal to or larger than the bandgap energy, ΔE_{bg}, it excites the electrons in the valance band to the conduction band, resulting in the formation of a positive hole (p^+) in the valance band and an electron (e^-) in the conduction band. The process of transfer of electron from the semiconductor to the adsorbate is called the reduction mechanism and the process of transfer of electron from the adsorbate to the semiconductor is called the oxidation mechanism. These processes are described illustratively in Figure 5.3. The positive hole oxidizes either pollutant directly or water to produce OH^- radicals, whereas the electron in the conduction band reduces oxygen adsorbed to photocatalyst (ZnO). In the photocatalysis with ZnO under aerated conditions, active oxygen species such as superoxide radical ($^{\bullet}O_2^-$), hydroxyl radical ($^{\bullet}OH$), and hydrogen peroxide (H_2O_2) have been noticed as key species to initiate the reactions [40–41]. These species are produced photocatalytically as shown by the following equations [42].

The photocatalytic process begins with absorbtion of photon.

$$ZnO + h\upsilon \longrightarrow (ZnO)\ e^- + h^+ \qquad (5.1)$$

Reactions involving conduction band e^- are

$$ZnO(e^-) + O_2 \longrightarrow ZnO + {}^{\bullet}O_2^- \qquad (5.2)$$

$$ZnO(e^-) + {}^{\bullet}O_2^- + 2H^+ \longrightarrow ZnO + H_2O_2 \qquad (5.3)$$

$$ZnO(e^-) + H_2O_2 \longrightarrow ZnO + {}^{\bullet}OH + OH^- \qquad (5.4)$$

$$^{\bullet}O_2^- + H_2O_2 \longrightarrow {}^{\bullet}OH + OH^- + O_2 \quad (5.4)$$

$$^{\bullet}O_2^- + H^+ \longrightarrow {}^{\bullet}HO_2 \quad (5.5)$$

$$ZnO(e^-) + {}^{\bullet}HO_2 \longrightarrow ZnO + HO_2^- \quad (5.6)$$

$$HO_2^- + H^+ \longrightarrow H_2O_2 \quad (5.7)$$

$$2\ {}^{\bullet}HO_2 \longrightarrow O_2 + H_2O_2 \quad (5.8)$$

Reactions involving valence band h^+ are

$$ZnO(h^+) + H_2O_{ads} \longrightarrow ZnO + {}^{\bullet}OH_{ads} + H^+ \quad (5.9)$$

$$ZnO(h^+) + 2\ H_2O_{ads} \longrightarrow ZnO + 2\ H^+ + H_2O_2 \quad (5.10)$$

$$ZnO(h^+) + OH^-_{ads} \longrightarrow ZnO + {}^{\bullet}OH_{ads} \quad (5.11)$$

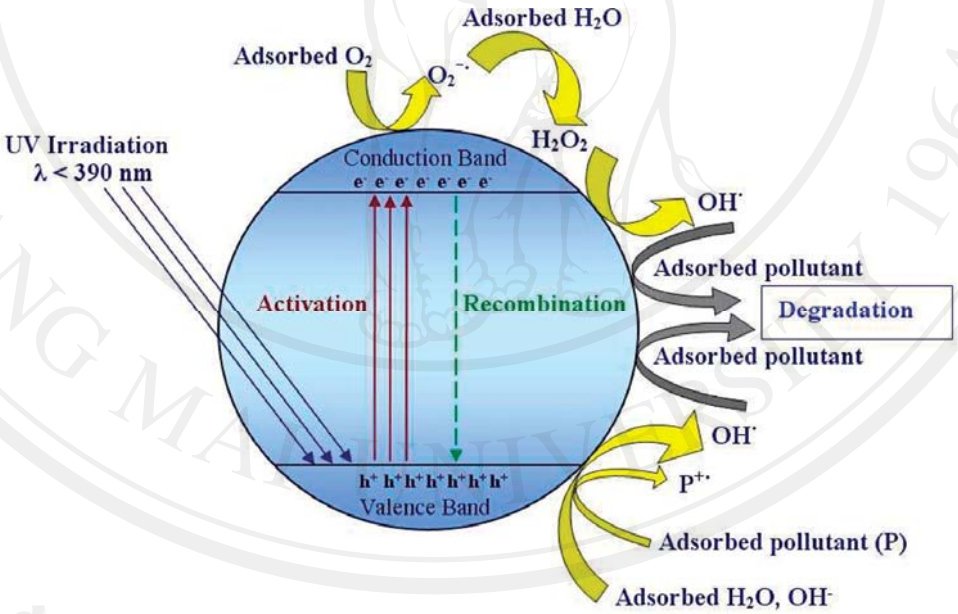

Figure 5.3 Schematic representation of the mechanism of photocatalytic activity. On absorption of photon of energy $h\upsilon$, electrons are excited from valence band (VB) to conduction band (CB). There is a transfer of electron to oxygen molecule to form superoxide ion radical ($^{\bullet}O^{-2}$) and a transfer of electron from water molecule to VB hole to form hydroxyl radical ($^{\bullet}OH$) [42].

The above-mentioned sequence of chain reactions describes more or less the biocidal activities when ZnO is exposed to UV radiation in the presence of H_2O and dissolved O_2. Thus, illuminated ZnO can decompose and mineralize organic compounds by participating in a series of oxidation reactions leading to carbon dioxide and water.

$$^{\bullet}OH + O_2 + \text{organic} \longrightarrow CO_2 + H_2O \qquad (5.12)$$

5.1.2 Photocatalytic oxidation [43]

The most powerful advanced oxidation systems are based on the generation of hydroxyl radicals. The hydroxyl radical is an extremely powerful oxidizion agent, second only to Fluorine in power (2.23 in relative oxidizing power). Table 5.1 shows the common chemical oxidants placed in the order of their oxidizing strength.

Table 5.1 The common chemical oxidants, placed in the order of their oxidizing strength.

Relative Power of Chemical Oxidation		
Compound	**Oxidation Potential (volts)**	**Relative Oxidizing Power (Cl_2 = 1.0)**
Hydroxyl Radical	2.8	2.1
Sulfate Radical	2.6	1.9
Ozone	2.1	1.5
Hydrogen Peroxide	1.8	1.3
Permanganate	1.7	1.2
Chlorine Dioxide	1.5	1.1
Chlorine	1.4	1.0
Oxygen	1.2	0.90
Bromine	1.1	0.80
Iodine	0.76	0.54

Utilizing the strong oxidation strength of hydroxyl radical, photocatalytic oxidation can effectively disinfect, deodorize, and purify air, water, and different surface area.

5.1.3 Photocatalytic reduction [44]

Photogenerated electrons at the conduction band of ZnO are relatively weaker reductants. However, the presence added electron donor as organic hole scavenger is important in photocatalytic reduction process because it can be enhanced the reaction. In addition, hole scavengers, or some organic compounds could form reducing intermediates upon reacting with the hydroxyl radicals which could enhance the reduction reactions [44].

5.1.4 Effect of surfuce area on photocatalytic activity [45]

In several photocatalytic reactions, a linear relation between the rate of photocatalytic reaction and amount of substrate(s) adsorbed on the surface of photocatalyst has been reported. When the Langmuirian adsorption isotherm was expected, this behavior was sometimes calls Langmuir-Hinshewood (L-H) mechanism even if only a kind of adsorbed substrate was assumed. Strictly speaking, however, this is wrong, because L-H mechanism involves the surface reaction of two kinds of adsorbed species, which is not realized in photocatalytic reaction systems. However, the linear relation can be rationalized by taking into account the reaction between e^- and/or h^+ with the surface-adsorbed substrate. When the specific surface area is increased, i.e., particle size is decreased, without changing the surface properties. If one assumes the enough (saturated) substrate is adsorbed on the surface, the rate should be enhanced. Of course, it is impossible to adapt a general kinetic consideration of ordinary thermal catalytic reaction, where the constant surface density of active sites makes the rate in proportion with the specific surface area, to

the photocatalytic reaction. In the photocatalytic reaction system, only a portion of the photocatalyst particles or an outer part of bulk materials can adsorb incident photons, and the remainder of the photocatalyst does not take part in the reaction. However, the total number of absorbed photons should be constant if a sufficient amount of photocatalyst absorb all the incident photons and, therefore, the total number of e^-–h^+ pairs is expected to be independent of specific surface area.

Large surface area with constant surface density of substrate leads to faster rate of e^- and h^+ reaction with substrates, because of the larger number of substrates surrounding the e^-–h^+ pairs.

5.1.5 Effect of electron-hole recombination on photo catalytic activity [45]

The rate of e^-–h^+ recombination must be an alternative decisive factor in photocatalytic activity, since the photogenerated e^-–h^+ pairs recombine to give no chemical reaction unless they react with the surface adsorbed substrate. Unlike the rate of reaction e^-–h^+, it is very difficult to evaluate the recombination rate directly. One of the most probable structural features related to e^-–h^+ recombination is crystallinity. It is assumed that the recombination occurs at crystal defects.

In fact, amorphous ZnO showed negligible photocatalytic activity, presumably due to the defects in the particles. Surface of crystal is, in a sense, a defective site where continuity of crystal structure is terminated, and thereby, the larger the surface area, the faster the recombination. Since the surface area also a positive influence, i.e., in a reversed, estimation of overall photocatalytic activity should be made carefully; when the surface reaction predominates the recombinate, the photocatalyst of larger surface area is better, and vice versa

5.1.6 Design of photocatalysts of high activity [45]

The structural characteristics, e.g., crystal structure, particle size, surface area, ect, of photocatalysts determine their photocatalytic activities. However, the relation between the physical properties and the photocatalytic activities is not so simple, and at least two parameters related to the surface reactions and recombination of e^-–h^+ must be optimized to obtain highly efficient semiconductor photocatalysts. The larger surface area and high crystallinity are minimum requisites of photocatalysts. This is based on the larger surface area corresponds to higher rate of surface reaction of e^- and h^+, and the high crystallinity, i.e., little crystal defects to slower rate of e^-–h^+ recombination. Of course, the enhancement of photocatalytic activity depends on many factors such as particle size, surface area, amount of OH surface groups, crystallinity, and band gap. However, the preparation method is one the most important parameters for the best photoactivity. Moreover, photoactivity of doping materials depending on the type of transition metal ions doping, calcination temperature and the concentration of transition metal ions as reported by many researchers [45].

5.1.7 Increasing efficiency by incorporation of metal nanoparticles [46–50]

Given that charge separation requires a great deal of effort, incorporation of metal nanoparticles (as well as increasing visible light activity) is to facilitate charge separation. One way of doing this is to incorporate noble metal nanoparticles such as silver or gold into the ZnO material. As an example, incorporation of a small amount of silver (1–5%) [60] results in increased efficiency in photocatalysis. Silver has a "Fermi level" or electron accepting region at an energy just below the conduction

band. Therefore, after light absorption and charge separation, the electron in the conduction band can be effectively trapped by the silver, while the hole oxidises water and forms hydroxyl radicals, without the threat of recombination. Various researchers [46–50] have shown that there is an optimum amount or "Goldilock's zone" of silver to add-just enough is needed so that there are silver sites dispersed through the material to rapidly trap electrons, but that too much silver may cover ZnO and prevent light absorption. In addition, too much silver may mean that the silver acts as a recombination site itself-essentially it will form a bridge between an electron and a hole.

The emission of ZnO can be interpreted as a measure of the recombination efficiency. Studies examining the emission of these metal oxides have demonstrated that the emission intensity reduces on increasing amounts of silver-indicating that the silver is trapping electrons and reducing electron-hole recombination, as indicated in the diagram below.

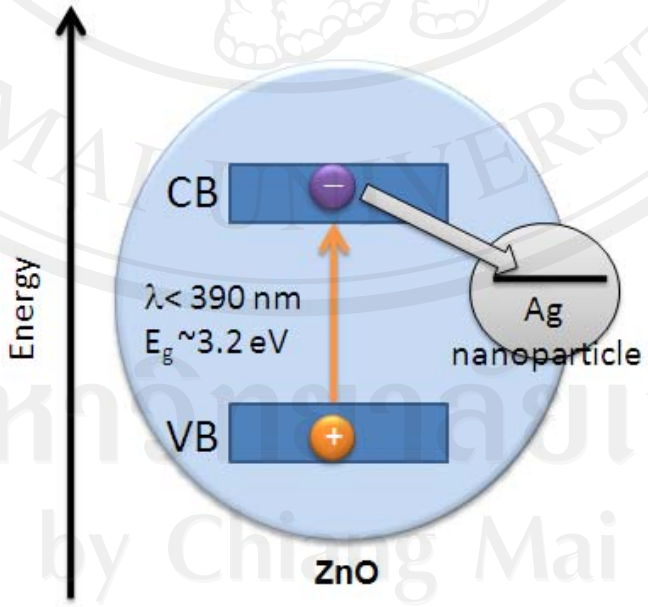

Figure 5.4 Incorporation of silver nanoparticles facilitate longer charge separation by trapping photogenerated electrons [51].

5.1.8 Literature review [52–60]

Photocatalytic activity based on pure ZnO and metal-doped ZnO have been investigated by many researchers.

The photocatalytic activity of Methyl orange (MO) and rhodamine 6G (R6G) in various semiconductors such as titanium dioxide (TiO_2), zinc oxide (ZnO), stannic oxide (SnO_2), zinc sulphide (ZnS) and cadmium sulphide (CdS) was investigated by Kansal et al. [52]. It was found that ZnO is the most active photocatalyst for decolorization of MO and R6G the decolorization of dyes is facilitated in the presence of catalyst and was favorable in basic region. The initial rate of photodecolorization increased with increase in catalyst dose upto an optimum loading. Further increase in catalyst dose showed no effect. Moreover, photocatalytic activity of ZnO is greater in the presence of solar light as compared to UV light.

Metal and metal oxide such as Ag, Pd, Fe, Cd, Nb and W had been shown to have a beneficial influence on the photoactivity of nanocrystalline semiconductor photocatalysts. The photocatalytic degradation of phenol solution using ZnO nanoparticles that were modified by depositing different amount of noble metal Ag or Pd on their surfaces with a photoreduction method was reported by Liqiang et al. [53]. The results showed that an appropriate amount of noble metal Ag or Pd modification could greatly enhance the photocatalytic activity of ZnO nanoparticles for degrading phenol solution. In addition, for 0.5 wt% noble metal deposited ZnO samples, the effects of Pd deposit were greater than that of Ag deposit, which was closely related to the increases in the surface hydroxyl content as well as charge separation rare.

Bailie et al. [54] reported the hydrogenation of but-2-enal over supported Au catalysts and characterization study using X-ray diffraction, infrared spectroscopy and

transmission electron microscopy. A series of ZnO supported Au catalysts with Au metal loadings of 0.25, 0.5, 1, 2, 5 and 10 wt%, were prepared by coprecipitation method. A mixed solution of $Zn(NO_3)_2.H_2O$ and $HAuCl_4.H_2O$, which contained the calculated amounts of the Zn and Au salts required to give the desired Au loading on ZnO, was heated to 80ºC. Au/ZnO catalysts were found to be selective for the formation of the unsaturated alcohol, but-2-en-1-ol rather than the saturated aldehyde, butanal. In general, the addition of thiophene was found to enhance the yield of the unsaturated alcohol. Detailed transmission electron microscopy and infrared spectroscopy studies showed that thiophene modification of Au/ZnO catalysts does not affect the Au-particle size or morphology; rather, thiophene undergoes irreversible dissociative adsorption giving a surface in which the Au sites are electronically promoted by sulfur. It is observed that thiophene modification does not give any marked effect on catalyst performance for the catalysts that contain large Au-particles (≥10 nm) and, hence, it was considered that the sulfur promotion observed was associated with smaller Au nanoparticles. The highest but-2-en-1-ol selectivities (~80%) were observed for 5 wt% Au/ZnO catalysts reduced at 400ºC prior to reaction. It was proposed that the origin of high selectivity is associated with large Au particles (10-20 nm in diameter) that were present in this catalyst.

Al-Sayari et al. [55] reported the preparation of Au/ZnO and Au/Fe_2O_3 catalysts using two coprecipitation methods. The important factors that control the synthesis of high activity catalysts for the oxidation of carbon monoxide at ambient temperature were investigated. The results presented in this study of the preparation of two materials Au/ZnO and Au/Fe_2O_3 showed that high activity materials for the oxidation of CO at ambient temperature could be readily prepared for both calcined

and non-calcined materials using two different coprecipitation procedures. These results were comparable with the results obtained from the standard catalysts supplied by the World Gold Council tested under the same reaction conditions. In particular, the factors involved in the preparation of catalysts which active without the need for a calcination step were evaluated. The two preparation methods differ in the manner in which the pH was controlled during the precipitation, either constant pH throughout or variable pH in which the pH was raised from an initial low value to a defined end point. Non-calcined Au/ZnO catalysts prepared using both methods were very sensitive to pH and ageing time. Catalysts prepared at a maximum pH = 5 with a short ageing time (ca. 0–3 h) exhibited high activity. Catalysts prepared at higher pH gave lower activity. However, all catalysts required a short operation period during which the oxidation activity increased. In contrast, the calcined catalysts were not particularly sensitive to the preparation conditions. Non-calcined Au/Fe_2O_3 catalysts exhibited high activity when prepared at pH ≥ 5. Calcined Au/Fe_2O_3 prepared using the controlled pH method retained high activity, whereas calcined catalysts prepared using the variable pH method were inactive. The study showed the immense sensitivity of the catalyst performance to the preparation methods. It was therefore not surprising that marked differences in the performance of supported Au catalysts for CO oxidation that were apparent in the extensive literature on this subject, particularly the effect of calcination, could be expected if the preparation parameters were not carefully controlled and reported.

Wu et al. [56] investigated the photocatalytic activities of the nc-Au/ ZnO nanorod composites in comparison with those of the ZnO nanorods and the ZnO film. The ZnO nanorods and the ZnO film were deposited on the Si substrates using

chemical vapor deposition. Photosynthesis of Au nanoparticles on the ZnO nanorods were conducted in $HAuCl_4$/ethanol solutions under 365 nm irradiation. The diameters and the densities of the Au nanoparticles formed on the surface of ZnO nanorods were tunable through varying the HAuCl4 concentration and the irradiation period. The enhancement of the photocatalytic activity for degradation of methyl orange (MO) was achieved by loading Au nanoparticles with sizes smaller than 15 nm on the ZnO nanorods and was more pronounced as the size of the Au nanoparticles was reduced to 5 nm. However, the photocatalytic activity of the nc-Au/ZnO nanorod composite was much lower than that of the ZnO nanorods when the diameter of the nc-Au was enlarged to 30 nm. The photocatalytic activity of the nc-Au/ZnO nanorods for degradation of MO was dependent on the diameter and the density of the nc-Au.

Zhou et al. [57] synthesized Ag/ZnO nano-composites via the coordination homogeneous co-precipitation method. The precursor was the mixture of Ag_2CO_3 and $Zn_5(OH)_6(CO_3)_2$. The particle size of the product increased with increasing calcining temperature and the dynamic growth index was 1.32. The photoreduction made Ag/ZnO and the Ag/ZnO photocatalyst prepared by the coordination homogeneous co-precipitation method were compared. The results of the photocatalytic degradation of methyl orange (MO) in aqueous solution indicated that the Ag/ZnO photocatalyst prepared by the coordination homogeneous co-precipitation method exhibited better photocatalytic performance than that prepared by the photoreduction method, especially the photocatalyst calcined at 300ºC, and the photocatalytic performance decreased when the calcining temperature increased from 300 to 700ºC.

The size of photocatalyst is one of the most important factors. Hariharan [58] compared the photocatalytic activity between bulk ZnO and ZnO nanoparticles, the results indicated that ZnO nanoparticles exhibited higher activity than bulk ZnO.

Moreover, the photocatalyst preparation process is another important factor. Wang et al. [59] compared photocatalytic activity of ZnO powder with various size scales (mean diameter size: 10, 50, 200 and 1000 nm) preparing by two different preparation processes as thermal evaporation process and chemical deposition process. ZnO nanoparticles with diameter size 50 nm prepared by thermal evaporation process showed the highest photocatalytic activity. However, the smaller 10 nm ZnO nanoparticles prepared by chemical deposition process showed the lower efficiency contrast to 200 nm ZnO powders prepared by thermal evaporation process, indicating that preparation process was the decisive factor rather than size and morphology.

The photocatalytic degradation of 10 ppm methylene blue (MB) solution that was used to evaluate the performance of FSP-made Ag-ZnO and compared to wet-made Ag-ZnO was reported by Height et al. [60]. The results showed that the photocatalytic activity of FSP-made Ag-ZnO was much better than that of wet-made Ag-ZnO. Moreover, FSP-made 3 at% Ag-doped ZnO exhibited the best photocatalytic performance. This result could be confirmed that the preparation process is very important factor for photocatalysts.

5.2 Chemicals and equipments

- Ethanol: C_2H_5OH (99.8% Lab-scan, MW. 46.1)
- Methanol: CH_3OH (99.8% Lab-scan, MW. 32.04)
- Glucose: $C_6H_{12}O_6$ (99% Ajax, MW. 180.16)
- Sucrose: $C_{12}H_{22}O_{11}$ (995 Ajax, MW. 342.3)
- Spiral photoreactor
- UV-lamp – NEC 20 watt T10 black light blue
- Solar light – Oceanlife, 50% natural daylight 6000K-50% actinic 03

blue, 18 watt

- Peristaltic pump – Masterflex Model 7553-79
- Conductivity meter – JENWAY 4330 and EUTECH PC 5500

5.3 Experimental

5.3.1 Calibration curve measurement

The spiral photoreactor was calibrated to obtain a relationship between the conductivity value and the amount of organic degraded. A suspension of Degussa P25 as a catalyst loading (1 g/L) was used during the calibration. The photocatalyst was circulated through the reactor and subjected to carbon burn off. After carbon burn-off, a known amount of carbon was added as sucrose (100–2000 μg of carbon) to the system and the lamp switched on. The conductivity value increased and the final conductivity reading was recorded as previous section which, corresponding to the known amount of carbon added. Calibration was relied on the establishing of the relation between carbon mass in the sample and the conductivity measurement values. For calculation, at the end of each run the recorded data which consisted of the increased in conductivity value was converted to the amount of carbon interpolated from the expression obtained from the calibration curve.

5.3.2 Preparation of photocatalyst suspension and operation

A schematic diagram of the spiral photoreactor was given in Figure 5.5. The spiral photoreactor consisted of (I) 70 cm long spiral reactor. The spiral reactor was made out of borosilicate glass tube with an outside diameter of 5 mm and the wall thickness of 1 mm. Photocatalytic reaction was initiated by illuminating the suspension inside the tube with (II) UV-lamp (NEC 18 watt T10 black light blue). The glass spiral filtered with the lamp was covered with aluminum foil to prevent

both the intrusions of ambient light and the emission of the harmful UV from the lamp. The attachments to the photoreactor were (III) a peristaltic pump (Masterflex Model 7553-79) (IV) a conductivity meter EUTECH PC 5500 and (V) a gas-liquid separator. All components were connected together using masterflex flexible tubing which was resistant to leaching of any organics.

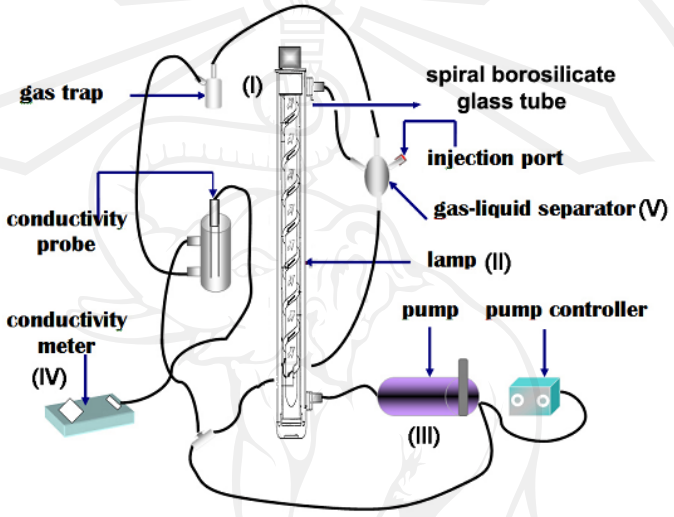

Figure 5.5 Schematic diagram of spiral photoreactor.

A 50 mL suspension of pure ZnO and Nb-doped ZnO nanoparticles having a loading of 1 g/L was prepared and its pH was about 7.0. The suspension was dispersed in an ultrasonic bath for 20 min before it was discharged into the spiral photoreactor. The suspension was circulated through out the spiral photoreactor. The suspension was subjected to a "carbon burn off" period, when it was illuminated to remove any contaminants adsorbed on the photocatalyst surface. The carbon dioxide generation was monitored using the conductivity meter (IV) in unit μS/cm. During carbon burn off, the conductivity reading increased to a constant value which was an indicating or that all impurities were removed. The system was then slowed to equilibrate at ambient atmospheric conditions by opening a valve at an exit port of a gas liquid separator (V).

Various organic carbon load (500 μg of carbon (500 μg C)), as glucose, sucrose, ethanol and methanol were injected into photocatalyst suspension through the inlet port (V). The catalyst-organic substrate mixture was circulated for 5 min without light illumination to ensure dispersion of the organic compound throughout the slurry. The lamp was then switched on. Subsequently, the increase in conductivity value was recorded every 1 second until the reaction ended. At the end of the photoreaction, the lamp was switched off and the system was flushed several times with Milli-Q water. All experiments were repeated at least twice.

5.4 Results and discussion

The 50% mineralization rate of methanol, ethanol, sucrose and glucose as a function amount of Nb loading using pure and Nb-doped ZnO nanoparticles photocatalyst containing 0.25, 0.50, 0.75 and 1.00 mol% Nb were shown in Figures 5.6–5.9 respectively.

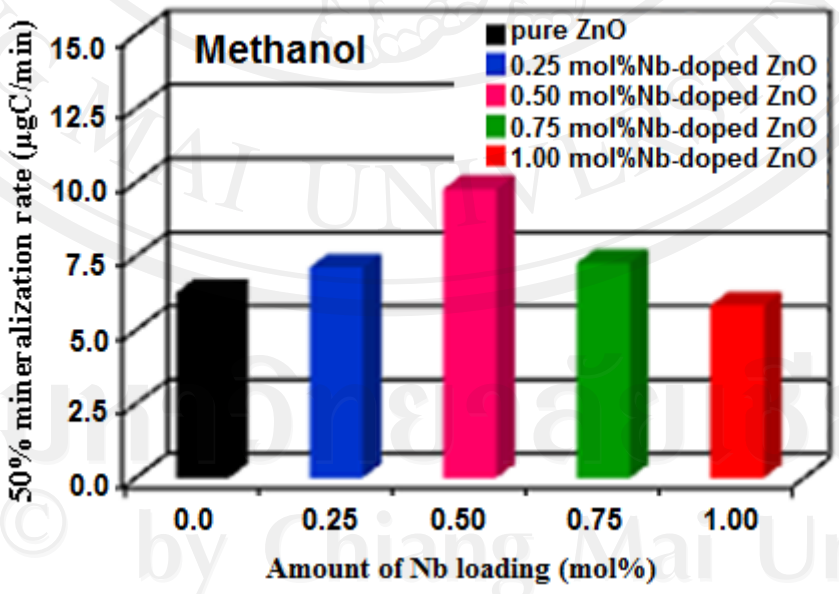

Figure 5.6 Photocatalytic degradation rate of methanol on pure ZnO and Nb-doped ZnO nanoparticles with different Nb loading.

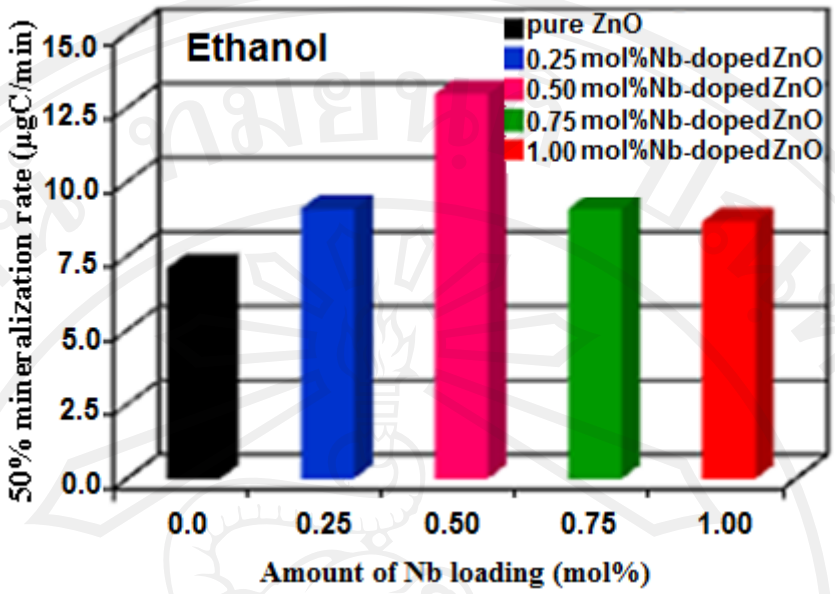

Figure 5.7 Photocatalytic degradation rate of ethanol on pure ZnO and Nb-doped ZnO nanoparticles with different Nb loading.

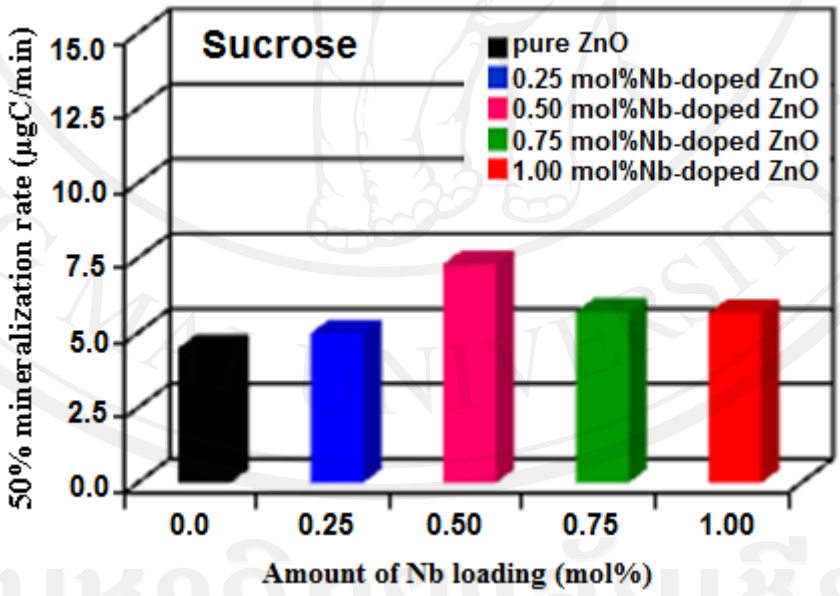

Figure 5.8 Photocatalytic degradation rate of sucrose on pure ZnO and Nb-doped ZnO nanoparticles with different Nb loading.

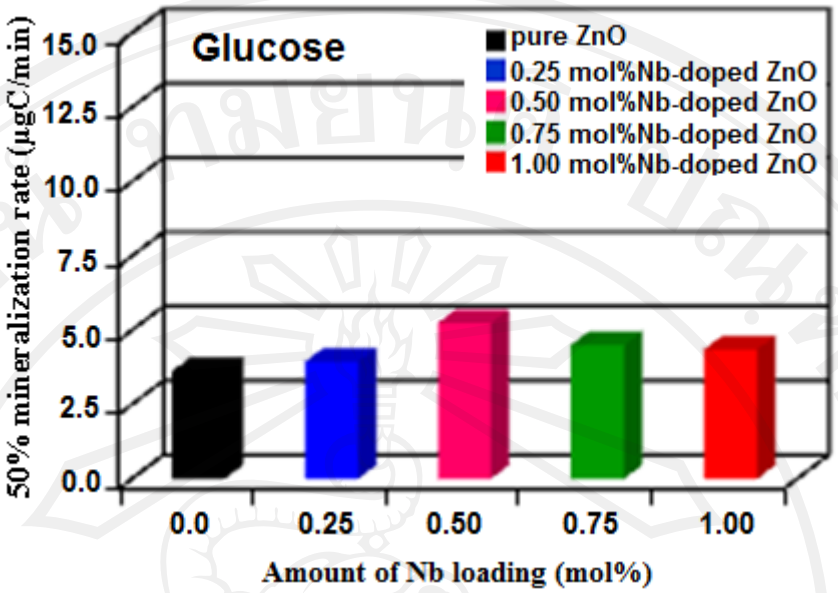

Figure 5.9 Photocatalytic degradation rate of glucose on pure ZnO and Nb-doped ZnO nanoparticles with different Nb loading.

It can be seen from Figures 5.6–5.9 and Table 5.2 that 0.50 mol % Nb-doped ZnO shows the highest photocatalytic activity among all samples and took shortest time to complete methanol, ethanol, sucrose and glucose degradation processes. The results clearly suggested that the photocatalytic activity of ZnO nanoparticles is greatly improved by doping an appropriate amount of Nb. The optimal amount of Nb was found to be 0.50 mol% for degradation of all organic compounds tested in this research. An enhanced photocatalytic activity of Nb-doped ZnO nanoparticles compared with that of the pure ZnO nanoparticles could be ascribed to Nb particles acting as electron traps, retarding the recombination of electron-hole pairs, and thus, promoting the photocatalytic activity. If the amount of Nb loading is higher than the optimal value, the activity of ZnO nanoparticles will begin to go down inversely. This is probably because an excess amount of Nb may become the center for recombining photoinduced electron and hole pairs.

Table 5.2 The comparison of time for completing the degradation process of methanol, ethanol, glucose and sucrose of different types of photocatalyst.

Photocatalyst type	Completed Methanol degradation time (min)	Completed ethanol degradation time (min)	Completed sucrose degradation time (min)	Completed glucose degradation time (min)
Pure ZnO	39.9	35.2	55.8	69.1
0.25 mol% Nb-doped ZnO	35.1	27.5	50.2	63.5
0.50 mol% Nb-doped ZnO	25.6	19.3	34.3	47.6
0.75 mol% Nb-doped ZnO	34.4	27.5	43.9	55.5
1.00 mol% Nb-doped ZnO	42.8	28.9	44.1	57.5

5.5 Conclusions

Nb-doped ZnO nanoparticles were successfully synthesized via the FSP technique by using zinc naphthenate and niobium (V) ethoxide as precursors in ethanol. The particle size of Nb-doped ZnO nanoparticles was found to decrease with increasing the Nb content. The photocatalytic activity of Nb-doped ZnO nanoparticles containing 0.25, 0.50, 0.75 and 1.0 mol% were investigated by UV-induced degradation of ethanol, methanol, sucrose and glucose in aqueous solution in the photocatalytic reactor. The results showed that the appropriate amount of Nb loading could greatly enhance the photocatalytic activity of ZnO nanoparticles for degrading ethanol, methanol, sucrose and glucose. An appropriate amount of Nb loading (0.50

mol%) over ZnO nanoparticles could greatly enhance the photocatalytic degradation of all organic compounds tested in this study. The photocatalytic activity under UV illumination of 0.50% Nb-doped ZnO on the organic compounds could be ranged in the following order Ethanol > Methanol > Sucrose > Glucose. This improved activity could be due to Nb particles acting as electron traps, retarding the recombination of electron-hole pairs, and thus, promoting the photocatalytic activity.

REFERENCES

1. Byrappa K., Subramani A.K., Ananda S., Lokanatharai K.M., Sunitha M.H., Basavalingu B., Soga K., Impregnation of ZnO onto activated carbon under hydrothermal conditions and its photocatalytic properties, *J. Mater. Sci*., 2006, **4**, 1355–1362.
2. Hariharan C., Appl. Catal., Photocatalytic degradation of organic contaminants in water by ZnO nanoparticles, *Appl. Catal. A-Gen.*, 2006, **304**, 55–61.
3. Hong R., Pan T., Qian J., Li H., Synthesis and surface modification of ZnO nanoparticles, *Chem. Eng. J.*, 2006, **119**, 71–81.
4. Xu F., Zhang P., Navrotsky A., Yuan Z.Y., Ren T.Z., Halasa M., Su B.L., Enthalpies of Formation of CdSxSe1-xSolid Solutions, *Chem. Mater.* 2007, **19**, 5680–5686.
5. Hariharan C., Photocatalytic Degradation of Organic Contaminants in Water by ZnO Nanoparticles, *Appl. Catal. A-Gen*. 2006, **304**, 55–61.
6. Lu F., Cai W.P., Zhang Y.G., Synthesis and Structurally Enhanced Photocatalytic Performance, *Adv. Funct. Mater.*, 2008, **18**, 1047–1056.
7. Comparelli R., Fanizza E., Curri M.L., Cozzi P.D., Mascolo G., Agostiano A., UV-induced photocatalytic degradation of azo dyes by organic-capped ZnO nanocrystals immobilized onto substrates, *Appl. Catal. B-Environ*., 2005, **60**, 1–11.

8. Akyol A., Yatmaz H.C., Bayramoglu M., Photocatalytic decolorization of Remazol Red RR in aqueous ZnO suspensions, *Appl. Catal. B-Environ.*, 2004, **54**, 19–24.

9. Liu H.Q., Yang J.X., Liang J.H., Huang Y.X., Tangz C.Y., ZnO Nanofiber and Nanoparticle Synthesized Through Electrospinning and Their Photocatalytic Activity Under Visible Light, *J. Am. Chem. Soc*., 2008, 91, 1287–1291.

10. Daneshvar N., Salari D., Khataee A.R., Photocatalytic degradation of azo dye acid red 14 in water on ZnO as an alternative catalyst to TiO_2, *J. Photoch. Photobiol. A.*, 2004, **162**, 317–322.

11. Zhang F., Zhao J., Zang L., Shen T., Hidaka H., Pelizzetti E., Serpone N., Pho-toassisted degradation of dye pollutants in aqueous TiO_2 dispersion under irradiation by visible light, *J. Mol. Catal. A-Chem.,* 1997, **120**, 173–178.

12. Gonqalves M.S.T., Oliveira-Campos A.M.F., Pinto E.M.M.S., Plasência P.M.S., Queiroz M.J.R.P. Photochemical treatment of solutions of azo dyes containing TiO_2, *Chemosphere*, 1999, **39**, 781–786.

13. Hasnat M.A., Siddiquey I.A., Nuruddin A., Comparative photocatalytic studies of degradation of a cationic and an anionic dye, *Dyes Pigments*, 2005, **66**, 185–188.

14. Černigoj U., Štangar U.L., Trebše P., Krašovec U.O., Gross S., Photocatalytically active TiO_2 thin films produced by surfactant-assisted sol-gel processing, *Thin Solid Films*, 2006, **495**, 327–332.

15. Kusvurana E., Samil A., Atanur O.M., Erbatur O., Photocatalytic degradation kinetics of di- and tri-substituted phenolic compounds in aqueous solution by TiO_2/UV, *Appl. Catal. B-Environ.*, 2005, **58**, 211–216.

16. Yu H., Zhang K., Rossi C. Theoretical study on photocatalytic oxidation of VOCs using nano-TiO_2 photocatalyst. *J. Photoch. Photobiol. A*., 2007, **188**, 65–83.

17. Caliman A.F., Cojocaru C., Antoniadis A., Poulios I., Optimized photocatalytic degradation of Alcian Blue 8 GX in the presence of TiO_2 suspensions, *J. Hazard. Mater.*, 2007, **144**, 265–273.

18. Khodja A.A., Sehili T., Pilichowski J.F., Boule P., Photocatalytic degradation of 2-phenylphenol on TiO_2 and ZnO in aqueous suspensions, *J. Photoch. Photobiol. A*., 2001, **141**, 231–239.

19. Sakthivel S., Neppolian B., Shankar M.V. Arabindoo B., Palanichamy M., Murugesan V., Solar photocatalytic degradation of azo dye: comparison of photocatalytic efficiency of ZnO and TiO_2, *Sol. Energ. Mat. Sol. C.,* 2003, **77**, 65–82.

20. Hao Y., Yang M., Li W., Qiao X., Zhang L., Cai S., A photoelectrochemical solar cell based on ZnO/dye/polypyrrole film electrode as photoanode, *Sol. Energ. Mat. Sol. C.*, 2000, **60,** 349–359.

21. Lizama C., Freer J., Baeza J., Mansilla H.D., Optimized photodegradation of Reactive Blue 19 on TiO_2 and ZnO suspensions, *Catal. Today*, 2002, **76**, 235–246.

22. Daneshvar N., Salari D., Khataee A.R., Photocatalytic degradation of azo dye acid red 14 in water on ZnO as an alternative catalyst to TiO_2, *J. Photochem. Photobiol. A.*, 2004, **162**, 317–322.

23. Akyol A., Yatmaz H.C., Bayramoglu M., Photocatalytic decolorization of Remazol Red RR in aqueous ZnO suspensions, *Appl. Catal. B-Environ.*, 2004, **54**, 19–24.

24. Mrowetz M., Selli E., Photocatalytic degradation of formic and benzoic acids and hydrogen peroxide evolution in TiO_2 and ZnO water suspensions, *J. Photoch. Photobiol. A.*, 2006, **108,** 15–22.

25. Peng F., Wang H., Yu H., Chen S., Preparation of aluminum foil-supported nano-sized ZnO thin films and its photocatalytic degradation to phenol under visible light irradiation, *Mater. Res. Bull.*, 2006, **41**, 2123–2129.

26. Kansal S.K., Singh M., Sud D., Studies on photodegradation of two commercial dyes in aqueous phase using different photocatalysts, *J. Hazard. Mater.,* 2007, **141**, 581–590.

27. Linsebigler A.L., Lu G., Yates J.T., Photocatalysis on TiO_2 Surfaces: Principles, Mechanisms and Selected Results, *Chem. Rev.* 1995, **95**, 735–758.

28. http://www.eclogiteskincare.com/blog/ (December 12, 2010)

29. Tani T., L. Mädler, S.E. Pratsinis, Homogeneous ZnO Nanoparticles by Flame Spray Pyrolysis, *J. Nanopart. Res.*, 2002, **4**, 337–343

30. Marci G., Augugliaro V., Lopez-Munoz M.J., Martin C., Palmisano L., Rives V., Schiavello M., Tilley R.J.D., Venezia A.M., Preparation Characterization and Photocatalytic Activity of Polycrystalline

ZnO/TiO_2 Systems. 2. Surface, Bulk Characterization, and 4-Nitrophenol Photodegradation in Liquid−Solid Regime, *J. Phys. Chem.* B, 2001, **105**, 1033−1040.

31. Mahata P., Madras G., Natarajan S., New Photocatalysts based on mixed - metal Pyridine dicarboxylates, *J. Phys. Chem. B*, 2006, **110**, 13759−13768.

32. Qiu X.Q., Li G.S., Sun X.F., Li L.P., Fu X.Z., Doping effects of Co ions on ZnO nanorods and their photocatalytic properties, *Nanotechnology*, 2008, **19**, 215703−215810.

33. Ekambaram S., Iikubo Y., Kudo A., Combustion synthesis and photocatalytic properties of transition metal-incorporated ZnO, *J. Alloys Compd.*, 2007, **433**, 237−240.

34. Ullah R., Dutta J., Hazard J., Photocatalytic degradation of organic dyes with manganese-doped ZnO nanoparticles, *Mater*. 2008, **156**, 194−200.

35. Zhang Q., Fan W., Gao L., Anatase TiO"2 nanoparticles immobilized on ZnO tetrapods as a highly efficient and easily recyclable photocatalyst, *Appl. Catal. B-Environ*., 2007, **76**, 168−173.

36. Anandan S., Vinu A., Lovely K.L.P.S., Gokulakrishnan N., Srinivasu P., Mori T., Murugesan V., Sivamurugan V., Ariga K., *J. Mol. Catal. A-Chem.*, 2007, **266**, 149−157.

37. Li D., Haneda H., Haneda, Photocatalysis of Sprayed nitrogen-containing Fe_2O_3-ZnO and WO_3-ZnO composite powders in gas-phase acetaldehyde decomposition, *J. Photochem. Photobiol. A-Chem*., 2003, **160**, 203−212.

38. Ekambaram S., Iikubo Y., Kudo A., Combustion synthesis and photocatalytic properties of transition metal-incorporated ZnO, *J. Alloys Compd*. 2007, **433**, 237–240.

39. Sappideen S., *PhD. Dissertation*, UNSW, 2000.

40. Hoffmann M.R., Martin S.T., Choi W., Bahnemann D.W., Environmental Applications of Semiconductor Photocatalysis, *Chem. Re*v., 1995, **95**, 69–96.

41. Serpone N., Pelizzetti E., Hidaka H., In *Photocatalytic Purification and Treatment of Water and Air*; Elsevier London, 1993.

42. Banerjee S., Gopal J., Muraleedharan P., Tyagi A.K., Raj B., Physics and chemistry of photocatalytic titanium dioxide: Visualization of bactericidal activity using atomic force microscopy, *Curr. Sci. India*, 2006, **90**, 1378–1383.

43. http://anchorgeneraltrading.com/solar%20clean.html (December 12, 2010)

44. Teoh W.Y., Madler L., Beydoun D., Pratsinis S. E., Amal Rose. Direct (one-step) synthesis of TiO_2 and Pt/TiO_2 nanoparticles for photocatalytic mineralisation of sucrose. *Chem. Eng. Sci.*, 2005, **60**, 5852–5861.

45. Kaneko M., Okura I., *Photocatalysis*, Springer, New York, 2002.

46. Asahi R., Morikawa T., Ohwaki T., Aoki K., Taga Y., Visible-light photocatalysis in nitrogen-doped titanium oxides, *Science.*, 2001, **294**, 269–271.

47. Bahnemann D., Photocatalytic water treatment: solar energy applications, *Sol. Energy*, 2004, **77**, 445–459.

48. Nakamura R, Tanaka T, Nakato Y., Mechanism for visible light responses in anodic photocurrents at N-doped TiO_2 film electrodes, *J. Phys. Chem. B*, 2004, **108**, 10617–10620.

49. Seery M.K., George R., Floris P., Pillai S.C., Silver doped titanium dioxide nanomaterials for enhanced visible light photocatalysis, *J. Photoch. Photobiol A.*, 2007, **189**, 258–263

50. Georgekutty R., Seery M.K., Pillai S.C., A Highly Efficient Ag-ZnO Photocatalyst: Synthesis, Properties and Mechanism, *J. Phys. Chem. C*, 2008, **112**, 13563–13570.

51. Kansal S.K., Singh M., Sud D., Studies on photodegradation of two commercial dyes in aqueous phase using different photocatalysts. *J. Hazard. Mater.*, 2007, **141**, 581–590.

52. Liqiang J., Dejun W., Baiqi W., Shudan L., Baifu X., Honggang X., Jiazhong S., Effects of noble metal modification on surface oxygen composition, charge separation and photocatalytic activity of ZnO nanoparticles. *J. Mol. Catal. A-Chem.*, 2006, **244**, 193–200.

53. http://photochemistryportal.net/home/index.php/2009/09/30/metal-oxide photocatalysis/. (December 12, 2010)

54. Bailie J.E., Abdullah H.A., Anderson J.A., Rochester C.H., Richardson N.V., Hodge N., Zhang J.G., Burrows A., Kiely C.J., Hutchings G.J., Hydrogenation of but-2-enal over supported Au/ZnO catalysts, *Phys. Chem. Chem. Phys.*, 2001, **3**, 4113–4121.

55. Al-Sayari S., Carley A.F., Taylor S.H., Hutchings G.J., Au/ZnO and Au/Fe_2O_3 catalysts for CO oxidation at ambient temperature: comments on the

effect of synthesis conditions on the preparation of high activity catalysts prepared by coprecipitation, *Top. Catal.*, 2007, **44**, 123–128.

56. Wu J., Tseng C., Photocatalytic properties of nc-Au/ZnO nanorod composites, Appl. Catal. B-Environ., 2006, **66**, 51–57.

57. Zhou G., Deng J., Preparation and photocatalytic performance of Ag/ZnO nano-composites, *Mater. Sci. Semicond. Process.*, 2007, **10**, 90–96.

58. Hariharan C., Photocatalytic degradation of organic contaminants in water by ZnO nanoparticles. *Appl. Catal. A-Gen.*, 2006, **304**, 55–61.

59. Wang H., Xie C., Zhang W., Cai S., Yang Z., Gui Y., Comparison of dye degradation efficiency using ZnO powders with various size scales. *J. Hazard. Mater.*, 2007, **141**, 645–652.

60. Height M.J., Pratsinis S.E., Mekasuwandumrong O., Praserthdam P., Ag-ZnO catalysts for UV-photodegradation of methylene blue. *Appl. Catal. B-Environ.*, 2005, **63**, 305–312.